Experimental demonstration of non-near-field image formed by negative refraction

Zhifang Feng,[1] Xiangdong Zhang,[2] Kun Ren,[1] Shuai Feng,[1] Zhi-Yuan Li,[1,*] Bingying Cheng,[1] and Daozhong Zhang[1]
[1]*Institute of Physics, Chinese Academy of Sciences, Beijing 100080, China*
[2]*Department of Physics, Beijing Normal University, Beijing 100875, China*
(Received 18 August 2005; revised manuscript received 23 January 2006; published 27 February 2006)

We have experimentally investigated the negative refraction and focusing by a two-dimensional photonic crystal (PC) made from a triangular lattice of metal-core dielectric-shell coated cylinders. At a certain frequency, the PC structure has an isotropic band at which the phase velocity is antiparallel to the group velocity. As a result, the PC structure can exhibit negative refraction and the corresponding effective refractive index can be close to the ideal value of −1. A flat lens formed from such a PC has been designed and its imaging properties have been investigated systematically. The measurement results show that the flat lens can form non-near-field images, and the source and image distance follow the conventional wave-beam negative refraction law for the refractive index of −1 irrespective of the slab thickness and the source distance.

DOI: 10.1103/PhysRevB.73.075118 PACS number(s): 78.20.Ci, 42.70.Qs, 41.20.Jb

I. INTRODUCTION

During the past few years, there has been a great deal of interest in studying the negative refraction of electromagnetic (EM) waves in the left-handed materials (LHMs) or photonic crystals (PCs).[1–20] The physical principles that allow negative refraction in the PCs arise from the dispersion characteristics of wave propagation in a periodic medium, which can be described by analyzing the equifrequency surface (EFS) of the photonic band structures.[6–20] The dispersion properties of the PC are determined by the lattice structure and various parameters of the system such as the dielectric constant contrast, size of the scatterers, and so on. Therefore, a wide variety of negative refraction phenomena and effects can be obtained by changing these parameters. Based on these phenomena, many high-technology applications have been proposed and demonstrated.[4,7,11–20]

It is well known that an important application of negative refraction materials is the flat lens.[1,4] Ideally, such a lens can focus a point source on one side of the lens into a real point image on the other side. It possesses some advantages over the conventional lens. For example, it can partly overcome the diffraction limit. Imaging behaviors against negative-refraction two-dimensional (2D) PC slab lenses have been observed by some authors via numerical simulations[13–15] and experimental measurements.[11] However, due to the anisotropy of the dispersion in 2D PCs, the images in many cases only appear in the near-field region and the dependence of the image distance on the source distance is weak.[13–15] In other words, the imaging does not obey the conventional refraction law of wave beams.

Recently, non-near-field imaging, which obeys fairly well the source and image distance relationship of a flat lens with an effective refractive index of $n=-1$, has been found theoretically in some specially designed 2D PCs.[16–20] However, to the best of our knowledge, the experimental demonstrations of such an interesting imaging behavior in PCs have not been reported. In this paper, we experimentally investigate the negative refraction and focusing by 2D PCs consisting of a triangular lattice of metal-core dielectric-shell coated cylinders. We will show that at a certain frequency the negative refraction with an effective refractive index of −1 can be realized. The flat lens can form non-near-field images and the source and image distance follow the conventional wave-beam negative refraction law.

The rest of the paper is arranged as follows. In Sec. II, we experimentally demonstrate the all-angle single-beam left-handed behaviors in the 2D triangular lattice PCs of coated cylinders. The frequency at which the effective refractive index is −1 has been determined. In Sec. III we systematically discussed the high-quality non-near-field imaging behaviors of the PC slab lens. The conclusions are given in Sec. IV.

II. NEGATIVE REFRATION IN 2D PC WITH TRIANGULAR LATTICE

We first investigate the left-handed behavior of EM waves in the triangular-lattice metallodielectric PC. The sample used in our experiments consists of a number of metal-core dielectric-shell coated cylinders immersed in a Styrofoam template. The PC structure has been investigated theoretically in Ref. 19. The radii of the metallic core and outer shell of the coated cylinder are $0.25a$ and $0.45a$, respectively, where a (=12 mm) is the lattice constant. The dielectric constant of the dielectric coating is 7.0. We use copper as the metallic core. In the experiments, we only consider the transverse magnetic (TM) modes (S wave), where the electric field is kept parallel to the extension axis of the cylinders.

In order to understand the transport properties of EM waves in the above structure, we first explore the transmission spectrum. A rectangular sample 110 mm thick and 400 mm wide was fabricated for microwave measurements. The measurements were carried out in a wide scattering chamber by using a N5230A vector network analyzer. The major component of the scattering chamber is two parallel metal plates in 1 cm separation. This geometry can faithfully model the physics of infinite 2D PC structures for the TM-polarized EM wave. The transmission data along the ΓK direction are plotted in Fig. 1(b). The calculated band structure of the PC structure is displayed for comparison in Fig. 1(a).

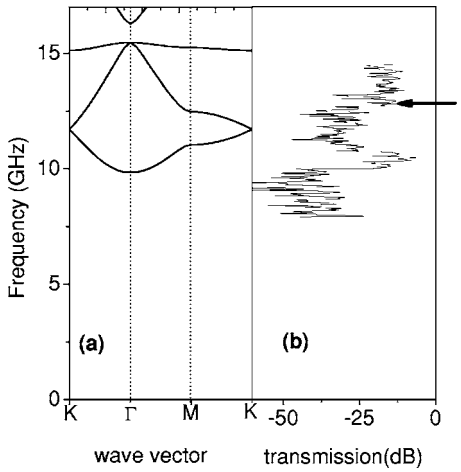

FIG. 1. (a) The calculated band structure of the coated-rod photonic crystals with triangular lattice for *S* wave. The radii of the inner core and outer shell of the coated cylinder are $0.45a$ and $0.25a$, respectively. Here $a=12$ mm. The dielectric constant of the outer dielectric coating is $\varepsilon=7.0$. (b) The measured transmission spectrum for the above sample along the ΓK direction. The arrow denotes the frequency 12.7 GHz where the negative refraction properties are investigated in this paper.

The calculations were performed by means of the multiple-scattering Korringa-Kohn-Rostoker method.[15,19] The Drude model is used to retrieve the dielectric constant of the copper core, similar to Refs. 15 and 19. From Figs. 1(a) and 1(b), we find an excellent agreement between the measurement and calculation results concerning the band gaps and pass bands positions. Both results show that the long-wavelength cutoff frequency of this metallodielectric sample is about 10 GHz.

The characteristic of the photonic band structures as shown in Fig. 1(a) suggests that we should focus on the second band in order to study the negative refraction problem of wave propagation in such a PC structure. The EFS contours of the system at several relevant frequencies in the second band are shown in Fig. 2. It is clear from the figure that the frequencies increase inwards, in other words, the EFS contours are concave. This means that the group velocities are opposite to the phase velocities. As a result, the transmission features of EM waves in the above PC structure

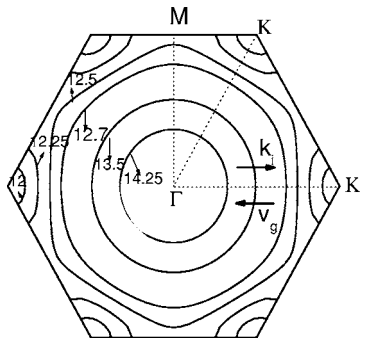

FIG. 2. Several equifrequency surface contours for *S* wave in the second band of the investigated 2D PC. The numbers in the figure mark the frequencies in unit of GHZ. k_i and V_g represent the wave vector and the group velocity, respectively.

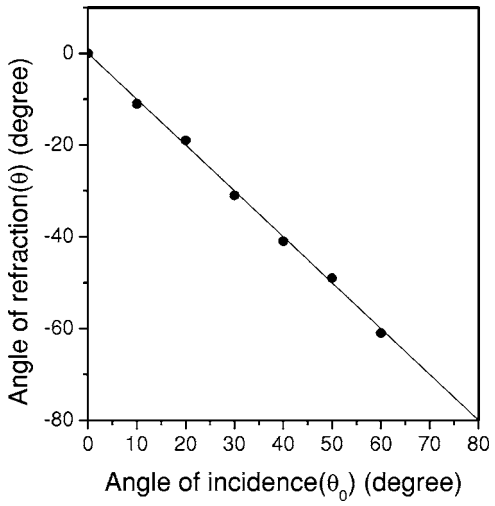

FIG. 3. The angles of refraction (θ) vs angles of incidence (θ_0) at the frequency 12.7 GHz for the *S* wave. Dark dots correspond to the measured results.

should exhibit a left-handed behavior. The direction of the refraction wave inside the PC slab can be estimated from the EFS. The frequency at which the corresponding effective refractive index of the PC structure is -1 is found to be 12.7 GHz.

In order to test experimentally the above theoretical analysis, we fabricated some wedge samples with different wedge angle θ_0. In experiment, the left surface of all the wedge samples was kept perpendicular to the incident direction to avoid multiple refraction, and the surface normal of the wedge interface was always set to be along the ΓK direction. A slit wave beam incident normal to the left surface of the sample, will transport along the ΓK direction until it meets the wedge interface of the sample. A part of the beam will refract out of the sample and the other is reflected back. The refraction wave either travels on the right side (positive refraction) or on the left side (negative refraction) of the surface normal. Therefore, by choosing different shapes of the wedge sample, we can extract the information of the refraction angle θ versus the incident angle θ_0. The refraction experiments were performed in a semicircular cavity. A dipole antenna was mounted on a goniometer that ran along the semicircular outer edge of the parallel plate waveguide to detect the refraction beam. The measurement results at the frequency of 12.7 GHz are summarized in Fig. 3 by the dark dots, while the solid line represents the theoretical results. Clearly the all-angle negative refraction has taken place at this frequency. More remarkably, θ is linearly proportional to θ_0 in the whole angle region. From the relationship between θ and θ_0, we can find that the negative refractive index of the system at this frequency is -1, which is close to the ideal LHM system that can serve as a flat superlens.[1,4]

III. NON-NEAR-FIELD IMAGE FORMED BY NEGATIVE REFRACTION

We now proceed to investigate the imaging effect of the flat lens to EM waves based on the above PC structure. A

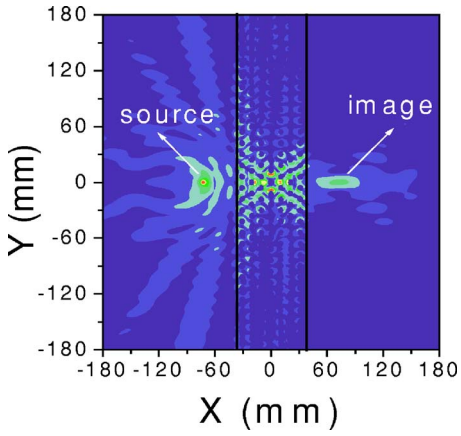

FIG. 4. (Color online) The intensity distribution of a point source and its image when the TM wave passes across the PC slab 75 mm thick at the frequency of 12.7 GHz. The two vertical lines represent the surfaces of the slab lens.

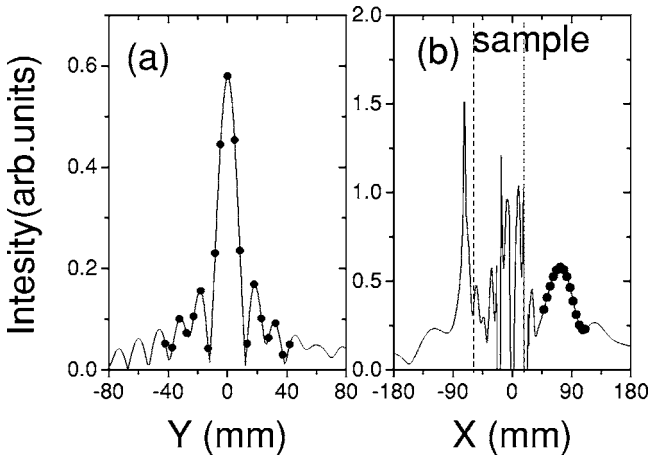

FIG. 5. The measured (dark dots) and calculated (solid lines) intensity distribution along the Y direction at the image plane located at $X=73$ mm (a), and along the X direction at the position $Y=0$ (b). Note that the experimental data have been normalized so that the maximum value is the same as the theoretical maximum intensity.

400 mm wide and 75 mm thick slab sample is taken as the first example. The surface normal of the slab is along the ΓK direction. A monochromatic point source radiating at the frequency of 12.7 GHz (corresponding to a wavelength of $\lambda = 23.6$ mm) was placed at a distance 37 mm (half thickness of the slab, corresponding to 1.6λ) away from the left surface of the slab. We first employed the multiple-scattering method[15,19] to calculate the propagation of the emitted wave across such a slab sample. A typical field intensity pattern for the TM wave passing through the slab is plotted in Fig. 4. X and Y represent the parallel and vertical directions of wave propagation, respectively. Only the data in a 360×360 mm domain around the sample center are displayed here. One can see a high quality image in the opposite side of the slab and the focusing of EM waves in the middle of the slab. The corresponding intensity distributions along the Y direction at the image place (located at $X=73$ mm) and the X direction at $Y=0$ are plotted in Figs. 5(a) and 5(b), respectively for clarity of view. Here and throughout this paper, the center of the slab is assumed to locate at $X=0$ and $Y=0$. A closer look at the data reveals that the transverse half widths of the central peaks are about 0.5λ, near the conventional diffraction limit. We have noticed that the summation of the source distance (U) and the image distance (V) is equal to the thickness of the slab (L).

We have carried out systematical experimental measurements to test the above theoretical observations. In the experiment, a monopole antenna was used as the point source. The monopole antenna is made from a coaxial cable where the inner conductor core (0.8 mm in diameter) is connected to a copper rod (about 3 mm in diameter and 1 cm in length) that is immersed into the chamber and serves as the emitter and receiver. The power distribution at the image place was measured by scanning and recording the transmission intensity along the line parallel to the surface of the slab at the focus point. The measurement results are shown as dark dots in Figs. 5(a) and 5(b). Excellent agreement between theory and experiment can be found clearly.

In order to see whether the summation of the source distance and the image distance is always equal to the thickness of the slab, we have checked a series of slab samples of different thicknesses. Figure 6(a) shows the calculated field pattern for a 115 mm thick sample. A monochromatic point source at 12.7 GHz was placed at a distance of half thickness of the sample (57 mm, or 2.4λ) away from the left surface of the slab and its image was found near the symmetric position in the opposite side of the slab. The experimental and simulation results of the power distribution at the image place are shown in Fig. 6(b). Excellent agreement between theory and experiment is also observed.

The above results are for the cases where the point sources are placed at the distances of half the thickness of the samples. We have considered more general situations by moving the light source and examining the relationship between the source distance and the image distance. Figure 7 shows the calculated field pattern for a 115 mm thick sample. A monochromatic point source radiating at frequency 12.7 GHz was placed at a distance 32 mm (1.4λ) from the left surface of the slab and its image was found in the opposite side of the slab. The image from the right side of the slab is 82 mm (3.5λ). The summation of the source distance and the image distance is near the thickness of the slab. The error is about ±5 mm.

We have considered more situations of the source distance. The results are given in Fig. 8 where the experiments were carried out for three different source distances, 32, 58, and 83 mm, corresponding to 1.4λ, 2.5λ, and 3.5λ. It can be found that although the image distance varies along with the source distance, the summation of them is always equal to the thickness of the slab. We have also checked more samples with different slab thicknesses L. The results of the dependence of $(U+V)/L$ on L are summarized in Fig. 9. It can be seen that the imaging behavior of the slab lens obeys fairly well the formula $U+V=L$. All these results clearly indicate that the imaging behavior of the negative refraction slab lens indeed follows the conventional refraction law of far-field focusing and imaging. This promising character is

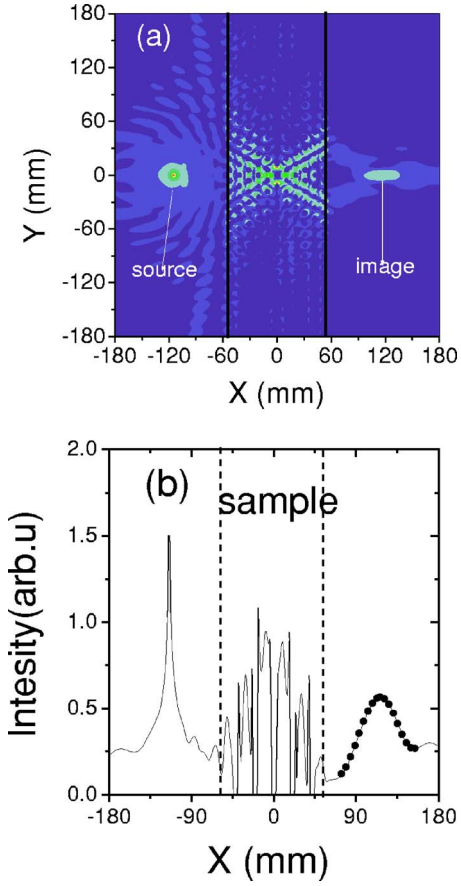

FIG. 6. (Color online) (a) The simulated intensity distribution of point source and its image against a PC slab 115 mm thick at the frequency of 12.7 GHz. The source distance is 57 mm. (b) The measured (dark dots) and calculated (solid lines) intensity distribution for the above sample along the X direction at the position $Y=0$. Note that the experiment data have been normalized so that the maximum value is the same as the theoretical maximum intensity.

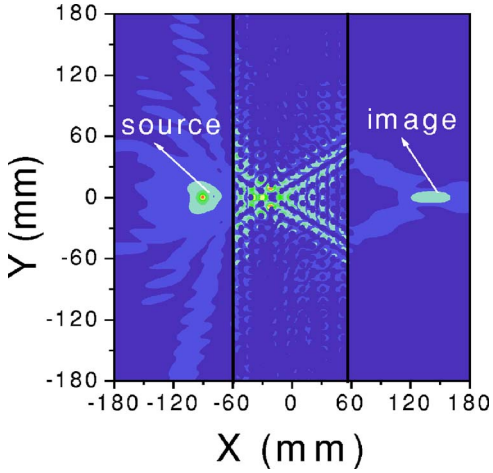

FIG. 7. (Color online) The intensity distribution of point source and its image against a PC slab 115 mm thick at frequency 12.7 GHz. The source distance is 32 mm.

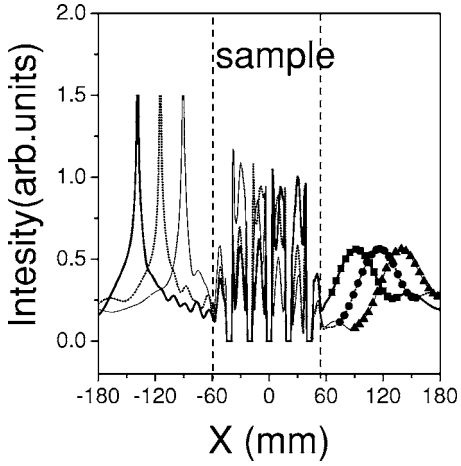

FIG. 8. The measured and calculated intensity distribution for the same sample with different distance of point source along X direction at $Y=0$. The distances of point source are 32 mm (thin solid line), 58 mm (short dots line), and 82 mm (thick solid line), respectively. The experimental results are corresponding represented by square, circular, and triangular dots, respectively.

possible only because the refractive index of our slab lens is identical to the ideal value of $n=-1$.

IV. SUMMARY

We have fabricated metallodielectric PCs consisting of the metal-core dielectric-shell coated cylinders arrayed in the triangular lattice and investigated systematically the negative refraction and focusing behavior of these PC structures. We have found that at a certain frequency the PC structure possess an isotropic band at which the phase velocity is antiparallel to the group velocity. As a result, the PC structure exhibits negative refraction and the corresponding effective refractive index is found to be close to the ideal value of −1. On the basis of such a PC structure, we have examined the imaging behavior of flat slab lens and found that non-near-field images can form against these slab lenses. In addition, we have systematically measured the relationship among the

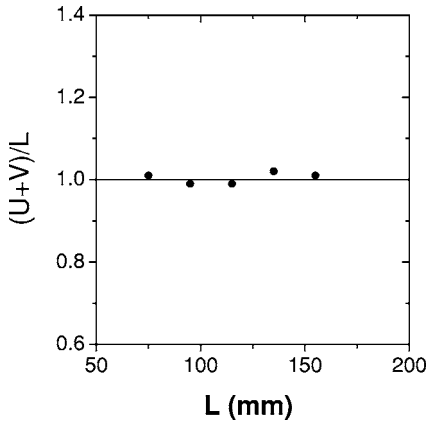

FIG. 9. Measured dependence of $(U+V)/L$ as a function of the thickness of the slab L.

source distance, image distance, and slab thickness for different slab samples, and found that the source distance and image distance sum up to a value identical to the slab lens within the experimental error irrespective of the slab thickness and the source distance. This clearly indicates that our designed PC lens is characteristic of a LHM lens with an effective refractive index of $n=-1$ and that the conventional refraction law of wave beam for focusing and imaging has been satisfied fairly well.

ACKNOWLEDGMENTS

This work was supported by the National Key Basic Research Special Foundation of China under Grant Nos. 2001CB610402 and 2004CB719804. X.Z. would like to thank the National Natural Science Foundation of China (Grant No. 10374009) and NCET. The support from the Supercomputing Centre, CNIC, and CAS is acknowledged.

*Email address: lizy@aphy.iphy.ac.cn

[1] V. G. Veselago, Sov. Phys. Usp. **10**, 509 (1968).
[2] D. R. Smith, W. J. Padilla, D. C. Vier, S. C. Nemat-Nasser, and S. Schultz, Phys. Rev. Lett. **84**, 4184 (2000).
[3] R. A. Shelby, D. R. Smith, and S. Schultz, Science **292**, 77 (2001).
[4] J. B. Pendry, Phys. Rev. Lett. **85**, 3966 (2000).
[5] Focus Issue "Negative refraction and metamaterials," Opt. Express **11**, 7 (2003).
[6] H. Kosaka, T. Kawashima, A. Tomita, M. Notomi, T. Tamamura, T. Sato, and S. Kawakami, Phys. Rev. B **58**, R10096 (1998).
[7] M. Notomi, Phys. Rev. B **62**, 10696 (2000).
[8] B. Gralak, S. Enoch, and G. Tayeb, J. Opt. Soc. Am. A **17**, 1012 (2000).
[9] C. Luo, S. G. Johnson, J. D. Joannopoulos, and J. B. Pendry, Phys. Rev. B **65**, 201104(R) (2002).
[10] E. Cubukcu, K. Aydin, E. Ozbay, S. Foteinopoulou, and C. M. Soukoulis, Nature (London) **423**, 604 (2003).
[11] P. V. Parimi, W. T. Lu, P. Vodo, and S. Sridhar, Nature (London) **426**, 404 (2003).
[12] E. Cubukcu, K. Aydin, E. Ozbay, S. Foteinopoulou, and C. M. Soukoulis, Phys. Rev. Lett. **91**, 207401 (2003).
[13] C. Luo, S. G. Johnson, J. D. Joannopoulos, and J. B. Pendry, Phys. Rev. B **68**, 045115 (2003).
[14] Z. Y. Li and L. L. Lin, Phys. Rev. B **68**, 245110 (2003).
[15] X. Zhang, Phys. Rev. B **70**, 205102 (2004); Appl. Phys. Lett. **86**, 121103 (2005).
[16] X. Wang, Z. F. Ren, and K. Kempa, Opt. Express **12**, 2919 (2004).
[17] A. Berrier, M. Mulot, M. Swillo, M. Qiu, L. Thylen, A. Talneau, and S. Anand, Phys. Rev. Lett. **93**, 073902 (2004).
[18] X. Hu and C. T. Chan, Appl. Phys. Lett. **85**, 1520 (2004).
[19] X. Zhang, Phys. Rev. B **70**, 195110 (2004); **71**, 165116 (2005); **71**, 235103 (2005); Phys. Rev. E **71**, 037601 (2005).
[20] Z. Feng, X. Zhang, Y. Q. Wang, Z. Y. Li, B. Y. Cheng, and D. Z. Zhang, Phys. Rev. Lett. **94**, 247402 (2005).